ACS APPLIED ENERGY MATERIALS

www.acsaem.org Article

All-Electrochemically Grown Sb_2Se_3/a-MoS_x Photocathodes for Hydrogen Production: The Effect of the MoS_x Layer on the Surface Recombination and Photocorrosion of Sb_2Se_3 Films

Magno B. Costa, Francisco W. S. Lucas, Marina Medina, and Lucia H. Mascaro*

Cite This: https://dx.doi.org/10.1021/acsaem.0c01413 Read Online

ACCESS | Metrics & More | Article Recommendations | Supporting Information

ABSTRACT: Sb_2Se_3 is considered a promising photocathode material for hydrogen production via solar water splitting. Nevertheless, losses caused by photocorrosion and slow charge transfer at the semiconductor/electrolyte interface require the presence of a cocatalyst to improve the kinetic factors. In this work, the activity of all-electrochemically grown Sb_2Se_3/amorphous-MoS_x photocathodes was studied in function of the number of cocatalyst deposition cycles. MoS_x, a noble-metal-free electrocatalyst, has shown high activity toward the hydrogen evolution reaction. It promoted an ∼70-time higher improvement in the photocurrent of the Sb_2Se_3-absorber. An antagonistic effect was observed as the number of cycles increased: thin MoS_x layers promoted the maximum enhancement in photocurrent and the decrease in surface recombination, but the photocorrosion inhibition was compromised. In the counterpart, thick MoS_x layers allowed the material to be less susceptible to photocorrosion, but the photocurrent was inhibited. Therefore, the relationship between cocatalyst thickness and photocurrent enhancement/inhibition, variation in surface recombination, and photocorrosion stability was evaluated.

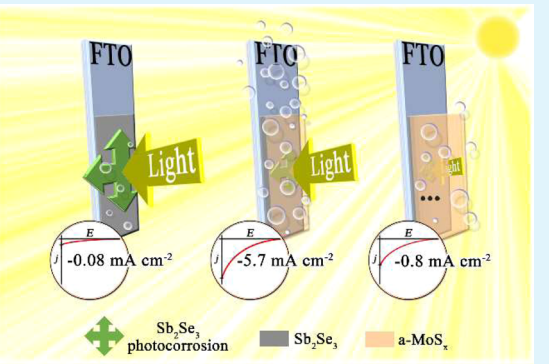

KEYWORDS: *antimony selenide, molybdenum sulfide, surface states, recombination, photocorrosion, photoelectrochemical hydrogen production*

Downloaded via UNIV FED DE SAO CARLOS on October 13, 2020 at 19:19:16 (UTC).
See https://pubs.acs.org/sharingguidelines for options on how to legitimately share published articles.

INTRODUCTION

Sb_2Se_3 thin films have been a new alternative for photovoltaic and photoelectrochemical devices based on low-cost absorber materials. These elements are earth-abundant and have low toxicity,[1] making their use as an absorber very attractive concerning the economic and environmental issues. In this scenario, Sb_2Se_3 has been presented as a promising photocathode for the hydrogen production via photoelectrochemical water splitting due to its adequate optical band gap energy (1.10−1.17 eV)[2,3] and high absorption coefficient (α = >10^5 cm^{-1})[4] in ultraviolet and visible light when compared with other commonly employed absorbers.[5−7] Additionally, its orthorhombic crystal structure formed by one-dimension parallel ribbons contributes to high anisotropic mobility of the carriers along them.[8,9] This may lead to photocurrent improvement if crystallographically textured toward an appropriate directions.[10]

However, the losses caused by Sb_2Se_3 photocorrosion, photoelectrochemical instability, and the slow charge transfer at the semiconductor/electrolyte interface have been limiting factors in achieving satisfactory and long-term light conversion efficiency.[11] The presence of a cocatalyst on its surface is indispensable for improving kinetic factors, and it reduces the effects that interfere with efficiency. The use of platinum and other platinum-group compounds as cocatalysts for hydrogen evolution reactions (HERs) has been widely used in various photoelectrochemical cell configurations for water splitting.[3,12] Nevertheless, this approach is not feasible on a commercial scale due to the rarity and high cost of these metals.[13] To overcome this economic issue, MoS_x (x = 2 and 3) is an electrocatalyst consisting of low-cost, nontoxic, earth-abundant elements.[14] Amorphous MoS_x (a-MoS_x) is reported as one of the major compounds for HERs because it has a high concentration of active sites at the edges layers, which favors its electrocatalytic activity if compared with its crystalline form.[15,16] Thus, the effects of a-MoS_x on Sb_2Se_3 thin films are of great importance for the evaluation of the photoelectrocatalytic and interfacial properties of the system.

In 2016, Britto et al. deposited MoS_2 layers on $GaInP_2$ from a Mo thin layer obtained using a sputter coater followed by

Received: June 16, 2020
Accepted: September 11, 2020
Published: September 11, 2020

© XXXX American Chemical Society

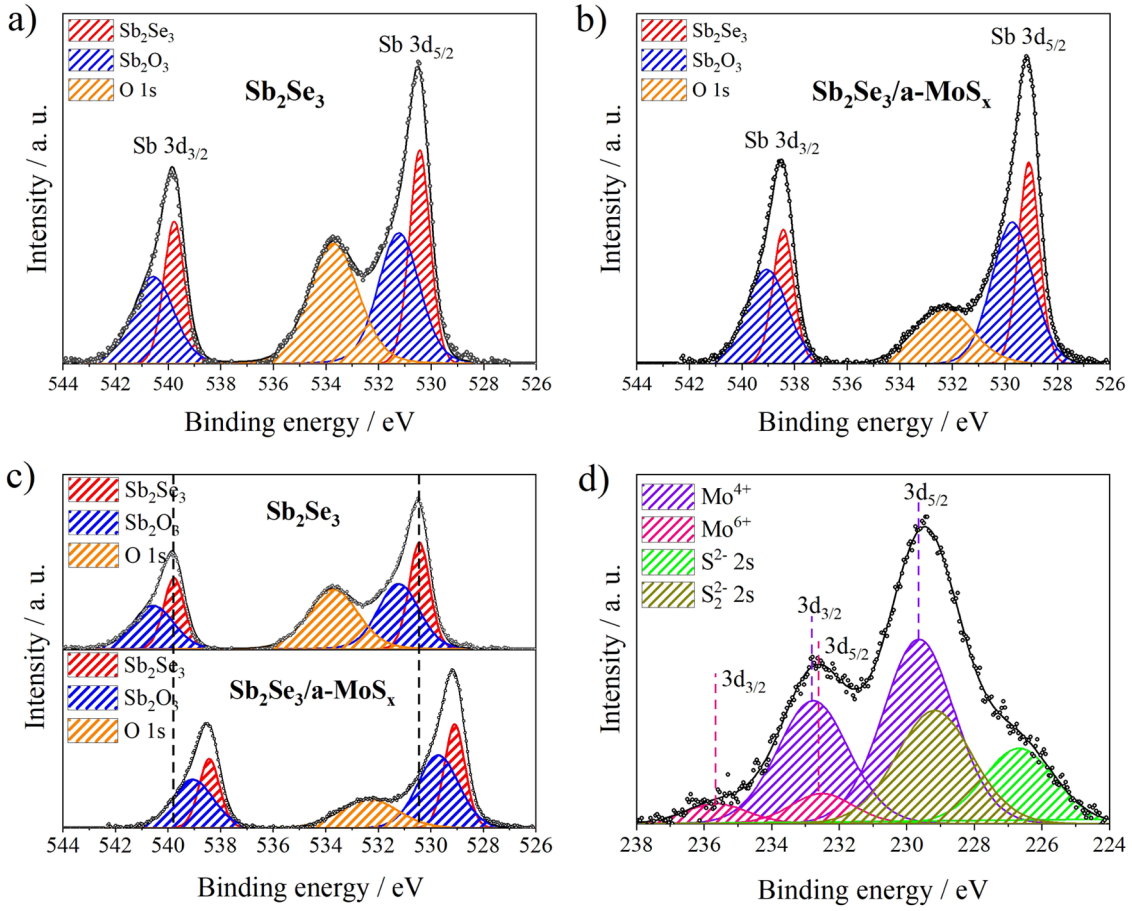

Figure 1. XPS spectrum for Sb 3d of (a) bare Sb_2Se_3 and (b) Sb_2Se_3/a-MoS_x films. (c) Displacement of the binding energy between (a) and (b). (d) XPS spectrum for Mo 3d and S 2s.

sulfurization in a tube furnace. The device showed that a very thin coating of MoS_2 provides stability to the $GaInP_2$ photocathode that is >90% of its initial value.[17] In an attempt to suppress the effects of photocorrosion, Prabhakar et al. electrodeposited a-MoS_x on sulfurized sputter-grown Sb_2Se_3 and achieved high catalytic performance and good stability without protective layers.[18] The low sulfurization temperature allowed for improvements in the potential onset and high photocurrent density. Tan et al. focused on a systematic study of the a-MoS_x deposition mechanism by cyclic voltammetry. They employed a protective layer of TiO_2 on Sb_2Se_3 and also achieved high photoelectrocatalytic performance.[19] Feng et al. expanded the use of MoS_x and employed it instead of Pt for the first time on Cu_2ZnSnS_4 (CZTS) photocathodes. From the configuration MoS_x−CdS/CZTS, they obtained a half-cell solar-to-hydrogen conversion efficiency of above 2.3% and excellent stability in neutral aqueous solution.[20]

In our work, Sb_2Se_3/a-MoS_x photocathodes were entirely grown by electrodeposition methods, and the effects related to the number of deposition cycles of the cocatalyst were evaluated. We have shown the importance of layer control in the a-MoS_x cocatalyst deposition on an Sb_2Se_3 absorber. In short, the cocatalyst provided a considerable reduction in charge transfer resistance at the semiconductor/electrolyte interface, while the thicker a-MoS_x layers minimized the photocorrosion effects of Sb_2Se_3. We also experimentally demonstrated that the presence of an a-MoS_x layer decreased the recombination on Sb_2Se_3 surface states and led to the reduction of Sb_2O_3 formed on its surface. An efficient charge transfer through the surface states was observed, so the a-MoS_x layer promoted an outstanding improvement in the photocurrent of the films. The stability of the cocatalyst was also evaluated in an acid medium, and the changes in the surface after the photoelectrochemical experiments were verified.

RESULTS AND DISCUSSION

MoS_x electrodeposition on the Sb_2Se_3 thin films was performed by cyclic voltammetry in a potential range between 0.1 and −1.0 V versus Ag/AgCl/$Cl^-_{(sat.\ KCl)}$. Figure S1 (available in the Supporting Information) shows the voltammetric profile for 15 cycles of deposition, where the processes involved in obtaining MoS_x can be more easily observed. The mechanism and the discussion about the voltammetric profile are included in the Supporting Information.

The surface micrographs of MoS_x-modified Sb_2Se_3 films as a function of the number of deposition cycles obtained using SEM are shown in Figure S2a. For all of the films, it is possible to observe agglomerated Sb_2Se_3 globules over the entire length of the samples. The surfaces of these globules are getting rugged as the number of deposition cycles increases (Figure S2a inset). This way, it is evident that MoS_x grows continuously and covers all the exposed Sb_2Se_3 surfaces. Moreover, there was no apparent degradation even after the deposition of MoS_x, as seen in Figure S3 (in the Supporting Information). To confirm that MoS_x is uniformly covering the

https://dx.doi.org/10.1021/acsaem.0c01413
ACS Appl. Energy Mater. XXXX, XXX, XXX−XXX

Table 1. Binding Energy of Components Deconvolved from the XPS Spectrum for the Bare Sb_2Se_3 and Sb_2Se_3/a-MoS_x

sample	(Sb_2Se_3) Sb^{3+} $3d_{5/2}$ / eV	(Sb_2O_3) Sb^{3+} $3d_{5/2}$ / eV	O 1s / eV	Mo^{4+} $3d_{5/2}$ / eV	Mo^{6+} $3d_{5/2}$ / eV	S^{2-} 2 s / eV	S_2^{2-} 2 s / eV
Sb_2Se_3	530.4	531.2	533.7				
Sb_2Se_3/a-MoS_x	529.1	529.7	532.3	229.6	232.5	226.6	228.2

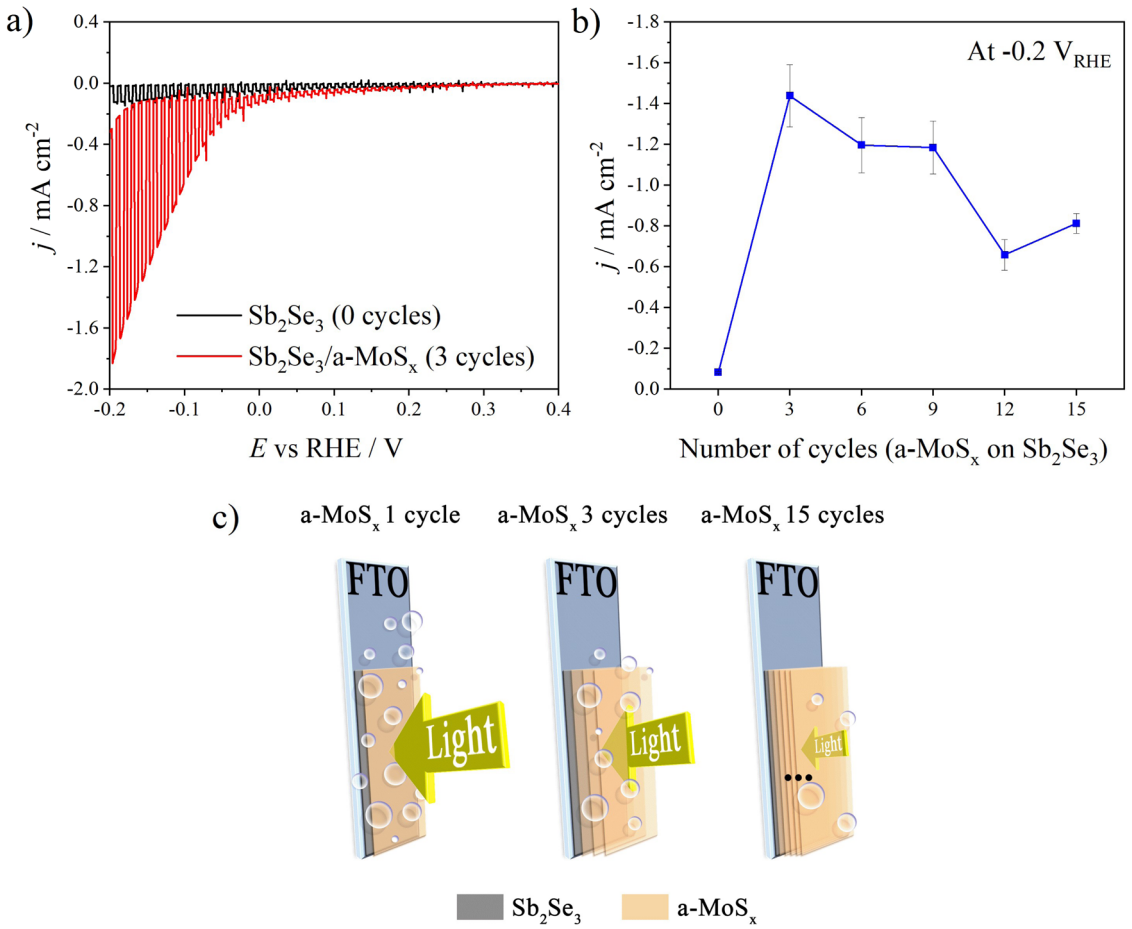

Figure 2. (a) Linear sweep voltammetry at 5.0 mV s^{-1} under solar illumination (100 mW cm^{-1}, AM 1.5G lens) with 1 s pulses in 1.0 mol L^{-1} H_2SO_4 for Sb_2Se_3 (0 cycle) and Sb_2Se_3/a-MoS_x (3 cycles). (b) Average of photocurrent values at −0.2 V_{RHE} of all films modified with a-MoS_x. (c) Schematic representation for different MoS_x deposition cycles on Sb_2Se_3 in the HER.

surface of Sb_2Se_3 films, EDS analyses were performed to verify the elemental distribution and to quantify the presence of each element (Figure S2b). It was observed that the potentiostatic electrodeposition followed by thermal treatment in a selenium atmosphere is a good method for obtaining stoichiometric films and the stoichiometry is not lost with MoS_x deposition. It is worth mentioning that, even though EDS is a semi-quantitative technique, several regions of the films were analyzed. In all cases, the analytical error was below 7% for Sb−Se elements (Figure S4 in the Supporting Information). For the MoS_x layer, this ratio has no significance to the desired end since the films obtained are amorphous and non-stoichiometric MoS_x as also reported in the literature.[15] However, the (Mo + S)/(Se + Sb) ratio shows that the amount of MoS_x deposited grows continuously as the number of deposition cycles increases.

Figure S5 (in the Supporting Information) shows the diffractogram of bare Sb_2Se_3 and Sb_2Se_3/MoS_x (15 cycles). The peaks indexed with "*" correspond to the fluorine-doped tin oxide (FTO) substrate pattern (cassiterite, JCPDS 41-1445). From the orthorhombic pattern of Sb_2Se_3 (JCPDS 89-821), it is possible to observe that all peaks between 2θ = 10° and 60° were indexed in both films and no secondary phases were observed even after the MoS_x deposition. Thus, it is possible to conclude that molybdenum sulfide is indeed nanocrystalline or amorphous (a-MoS_x).

For greater understanding about the chemical composition of the Sb_2Se_3 and a-MoS_x layers, XPS analyses were performed for bare Sb_2Se_3 and Sb_2Se_3/a-MoS_x. The XPS spectra can be seen in Figure 1, and the peak positions of Sb, O, Mo, and S are described in Table 1. Figure 1a,b corresponds to the Sb 3d and O 1s spectra with binding energies between 526 and 544 eV for bare Sb_2Se_3 and Sb_2Se_3/a-MoS_x, respectively. The separation between the peaks of the Sb 3d doublet pairs was maintained at 9.34 eV.[21] The presence of surface Sb_2O_3 is noted by the additional doublet with peaks at 531.2 and 540.6 eV. Sb_2O_3 is formed on the surface exposed to air as a result of the high Gibbs free energy and standard molar reaction enthalpy when compared with Sb_2Se_3.[22] It is likely that the oxide was not formed during the bulk electrodeposition, but only on the Sb_2Se_3 surface, since no Sb_2O_3 peak was observed in the XRD analyses. However, when the film is covered with

https://dx.doi.org/10.1021/acsaem.0c01413
ACS Appl. Energy Mater. XXXX, XXX, XXX−XXX

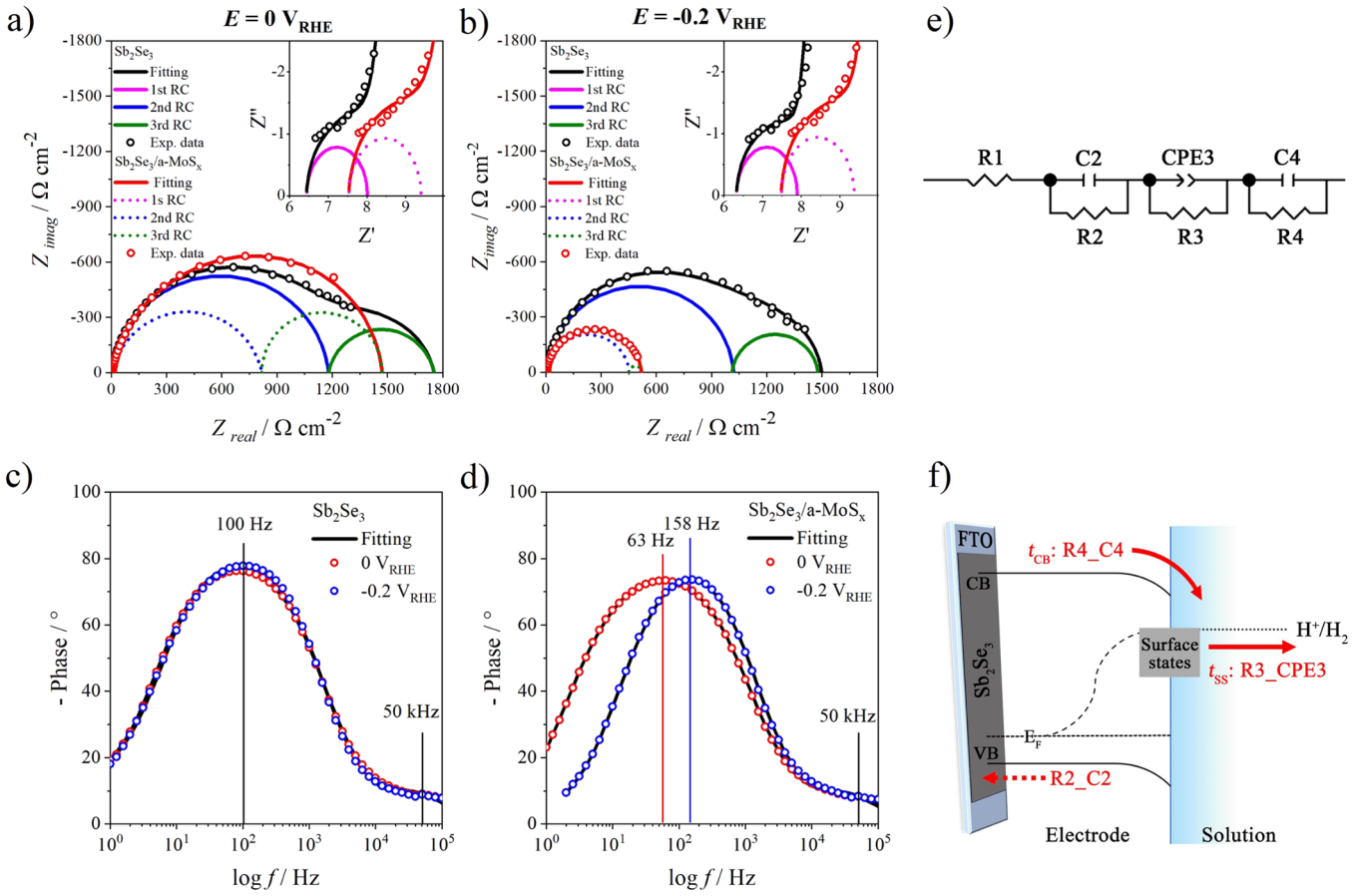

Figure 3. PEIS spectra for bare Sb_2Se_3 and Sb_2Se_3/a-MoS_x films at (a) 0 V_{RHE} and (b) −0.2 V_{RHE}, respectively. The inset highlights high-frequency regions. (c) and (d) Bode plots corresponding to (a) and (b) spectra for bare Sb_2Se_3 and Sb_2Se_3/a-MoS_x films, respectively. (e) Equivalent circuit used for fitting the PEIS spectra. (f) Schematic representation of the different charge transfer processes at the electrode/solution interface via surface states (t_{SS}) and conduction band minimum (t_{CB}).

MoS_x, a reduction in the area below the corresponding O 1s peak is noted. This is a result of the decrease in surface Sb_2O_3 formation due to the a-MoS_x coverage (more details will be shown later). Other evidence to ensure this assumption can be made by evaluating the areas of the Se spectra shown in Figure S6. The signal obtained is composed of two doublets of Se $3d_{5/2}$ and $3d_{3/2}$ (each one separated by an energy of 0.86 eV[21]), indicating the presence of Se^{2-} and Se^0. In addition, the presence of Se^0 is one piece of evidence that the surface of Sb_2Se_3 has been oxidized after being obtained. When evaluating their respective areas below the curve (Table S1 in the Supporting Information), the ratio between Se^{2-}/Se^0 increases for the Sb_2Se_3/a-MoS_x film, indicating that less Se^0 was formed and therefore less Sb_2O_3.

Figure 1c also shows the displacement of the Sb 3d and O 1s peaks toward a lower binding energy for the film covered with a-MoS_x. Therefore, the presence of MoS_x changes the Fermi level to less energetic regions, proving the formation of a more favourable Sb_2Se_3/MoS_x junction. The Mo 3d and S 2s spectra are shown in Figure 1d with binding energies between 224 and 238 eV, and the separation between the Mo 3d doublet peaks is at 3.13 eV.[21] For sulfur, it was necessary to have two S 2s singlets with chemical states of S^{2-} and S_2^{2-} for an acceptable adjustment of the data.[23] The molybdenum region can be deconvoluted into two different doublets that are equivalent to the Mo^{4+} and Mo^{6+} states, following the mechanisms provided in reactions 1, 2, and 3. In addition, the calculated Mo^{4+} percentage on the film surface, from its respective area below the curve, corresponds to 87.4% over 12.6% Mo^{6+} (Table S1 in the Supporting Information). This is a strong indication that MoS_2 electrodeposition is favored during cathodic scanning over MoS_3 formation in anodic scanning (seen previously in the cyclic voltammogram), as reported by Tan et al.[19]

Figure S7 (in the Supporting Information) shows the optical band gap energies obtained from the Tauc plot in a range of 1.0 to 1.5 eV for bare Sb_2Se_3 (0 cycles) films and those modified with a-MoS_x. The individual values for each film obtained with a different number of deposition cycles can be seen in the inset of Figure S7. Using techniques such as temperature-dependent transmission spectroscopy and temperature-dependent photoluminescence at 300 K,[4] Chen et al. obtained Sb_2Se_3 by thermal evaporation and reported its direct and indirect band gap energies in a range of 1.17 ± 0.02 and 1.03 ± 0.01 eV, respectively. In our case, for electrodeposited Sb_2Se_3 films, the indirect band gap value was 1.18 ± 0.01 eV for all films. In other words, there were no significant differences in the band gap energy between the bare Sb_2Se_3 (0 cycles) films and those modified with a-MoS_x, proving that the Sb_2Se_3 films are not doped during the deposition of the MoS_x layer.

The Mott−Schottky (M−S) analyses were performed to verify the band edge positions of Sb_2Se_3 films and to confirm if the material is suitable for the HER via photoelectrochemical water splitting. The M−S plots at different frequencies can be

https://dx.doi.org/10.1021/acsaem.0c01413
ACS Appl. Energy Mater. XXXX, XXX, XXX−XXX

Table 2. Resistance and Capacitance Values Based on Analog Equivalent Circuit Setting

sample	*R1* / Ω cm^{-2}	*C2* / μF s^{n-1} cm^{-2}	*R2* / Ω cm^{-2}	*CPE3* / μF s^{n-1} cm^{-2}	*R3* / kΩ cm^{-2}	*C4* / μF s^{n-1} cm^{-2}	*R4* / kΩ cm^{-2}	R_{Total} / kΩ cm^{-2}
Sb_2Se_3								
0 V_{RHE}	4.6	1.8	1.2	17.2 (n = 0.92)	1.4	448.0	0.5	1.9
−0.2 V_{RHE}	4.5	1.5	1.1	15.8 (n = 0.94)	1.4	217.0	0.5	1.7
Sb_2Se_3/a-MoS_x								
0 V_{RHE}	4.4	1.5	1.1	31.2 (n = 0.87)	0.8	48.7	0.6	1.4
−0.2 V_{RHE}	4.3	1.4	1.1	14.0 (n = 0.94)	0.4	34.5	0.1	0.5

seen in Figure S8a, and flatband potentials (E_{fb}) are inserted in the graphs. For comparisons, theoretical bulk MoS_2[24] was added to the scheme in Figure S8b. In the analyzed film, the conduction band energy is more energetic than the thermodynamic potential of hydrogen reduction at pH 0 (−4.0 eV ± 0.05) and, together with MoS_2, makes this system a suitable photocathode for the H_2 gas evolution reaction.

The photoelectrochemical measurements were performed in an electrolyte solution of 1.0 mol L^{-1} H_2SO_4. The photocurrent density was obtained by light and dark linear sweep voltammetry (LSV) with 1 s pulses in a potential range from open circuit potential to 200 mV more negative than the hydrogen thermodynamic potential (i.e., from ∼0.4 to −0.2 V_{RHE}). The LSV of the bare Sb_2Se_3 (0 cycles) and Sb_2Se_3/a-MoS_x (3 cycles) films can be seen in Figure 2a, while the LSV for other films can be seen in Figure S9 (in the Supporting Information). The average photocurrent density values obtained at −0.2 V_{RHE} can be seen in Figure 2b. It can be observed that all a-MoS_x-modified films have higher photocurrents than the Sb_2Se_3 (0 cycle) film due to their better electrocatalytic activity toward the HER.[25] It is well known that the use of a cocatalyst, such as a-MoS_x, reduces the activation energy and facilitates the charge transfer at the semiconductor/electrolyte interface, which led to increased photocurrent densities.[26,27] However, since the a-MoS_x layer becomes thicker as the number of deposition cycles increases, the photocurrent values decrease. This effect is in part due to parasitic light absorption, the higher coverage of an absorbent material (Sb_2Se_3) by a black nonphotoactive (a-MoS_x) one. To reinforce this assumption, an increase in the absorption coefficient is observed in Figure S7 in near-IR regions as the number of deposition cycles increases. This indicates that a greater amount of MoS_x deposited allows a greater effect of parasitic light absorption. Although for 3 to 9 cycles of deposition it is a slight change, for 12 and 15 cycles, the absorption is better observed. Thus, the higher average photocurrent value was obtained for the Sb_2Se_3/a-MoS_x (3 cycles) film, exhibiting a −1.4 mA cm^{-2} photocurrent density from the LSV at −0.2 V_{RHE}. Subsequently, an Sb_2Se_3/a-MoS_x (1 cycle) film was made to verify the trend observed in Figure 2b. A significant increase in photocurrent density was observed compared with Sb_2Se_3/a-MoS_x (3 cycles) films, exhibiting an initial value of −5.7 mA cm^{-2}, that is, ∼70 times higher than bare films (Figure S10a in the Supporting Information). This may indicate that thinner layers of a-MoS_x allow more light to reach Sb_2Se_3 and generate more e^-/h^+ couple for water splitting. However, the greater amount of exposed Sb_2Se_3 made the film be more susceptible to photocorrosion and the photocurrent quickly decreased to values below those presented by the Sb_2Se_3/a-MoS_x (3 cycles) film, as seen in Figure S10b (in the Supporting Information). A schematic representation can be seen in Figure 2c to demonstrate the trend of the photocurrent observed in the films obtained from 1, 3, and 15 deposition cycles of the cocatalyst.

It is very interesting to note that the photocurrent density values at 0 V_{RHE} for the Sb_2Se_3 (0 cycles) and Sb_2Se_3/a-MoS_x (3 cycles) films do not differ significantly, requiring a higher overpotential to activate the effect of the cocatalyst on the charge transfer in the HER. To characterize the charge transfer phenomena, photoelectrochemical impedance spectroscopy (PEIS) was performed to check the charge transfer resistance for each of the transfer mechanisms present in the system. The experiments were done under simulated solar illumination in a frequency range from 0.1 Hz to 100 kHz, polarized at 0 and −0.2 V_{RHE} for both films. Figure 3a,b shows the Nyquist plots for the Sb_2Se_3 and Sb_2Se_3/a-MoS_x films, respectively. From the graphs, three semicircles could be adjusted in the spectra to allow better fitting of the data in all films. In Figure 3c,d, the Bode diagram shows two regions with different frequencies, one of them at high frequencies (∼50 kHz) and the other at medium frequencies (∼100 Hz). The dominium at the medium frequencies is composed of two independent processes with close time constants. Thus, as seen in Figure 3e, it was inferred that the equivalent circuit for the films is composed of three connected series of resistor−capacitor models: a resistor and capacitor for the first and third semicircles, and a resistor and constant phase element (CPE) for the second semicircle, in addition the presence of the ohmic resistance of the solution (R1).

Bertoluzzi and Bisquert formulated an equivalent circuit analytical model for semiconductors applied to water splitting and related that interfacial kinetics could be described by three arcs in the Nyquist plot.[28] The same model can be adopted to describe the interfacial kinetics behavior of the films in this work. Although the first semicircle at high frequencies of the Bertoluzzi and Bisquert model be assigned to the transfer via trapping/detrapping of the charge carriers ($t_{T/D}$), this was not possible in the circuit obtained in this work. In this case, RC circuits at high frequencies (R2 and C2) with low resistance can be assigned to the bulk and the FTO/Sb_2Se_3 interface, as previously observed by Morante and co-workers.[29] The second semicircle at medium frequencies (R3 and CPE3) represents the charge transfer through surface states (t_{SS}).[19,30] Finally, the last one at low frequencies (corresponding to R4 and C4) is related to the direct charge transfer from the conduction band minimum to the electrolyte (t_{CB}). A summary of the previous discussion can be seen in the schematic representation in Figure 3f.

For the quantitative analysis of the model, the resistance and capacitance values are summarized in Table 2. Also, the errors attributed to each element are shown in Figure S11 (in the Supporting Information). In all cases, both the resistance of solution and that related to the FTO/Sb_2Se_3 interface have low values. Regarding t_{SS} resistance, Sb_2Se_3/a-MoS_x films show a reduction in R3 when compared with those in the absence of

https://dx.doi.org/10.1021/acsaem.0c01413
ACS Appl. Energy Mater. XXXX, XXX, XXX−XXX

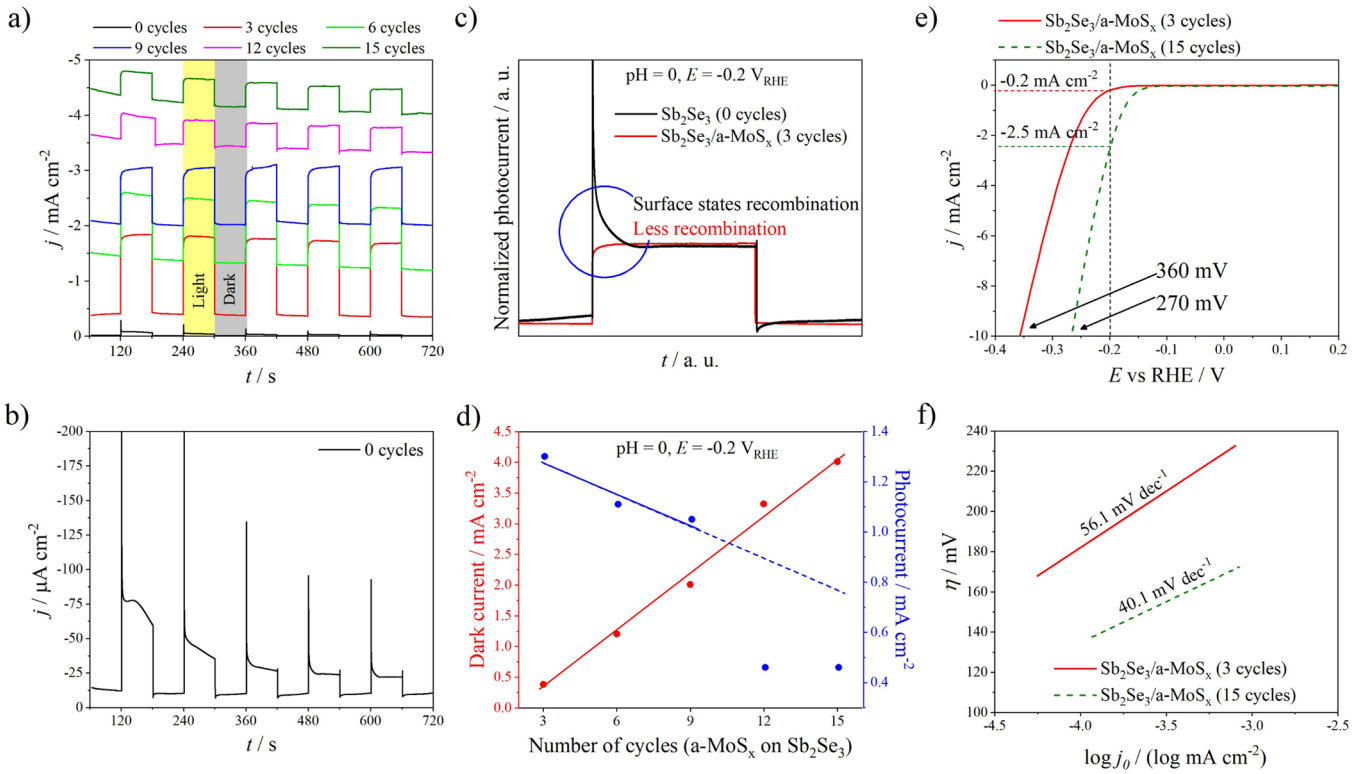

Figure 4. (a) Photocurrent transients of bare Sb_2Se_3 and Sb_2Se_3/a-MoS_x films with $E = -0.2$ V_{RHE} and 60 s pulses in light and dark; (b) readjusted scale for bare Sb_2Se_3 films. (c) Analyses of the photocurrent decay for bare Sb_2Se_3 and Sb_2Se_3/a-MoS_x and (d) dark and photocurrent values from transient last pulse. (e) Polarization curves in dark and (f) Tafel plot for Sb_2Se_3/a-MoS_x obtained from 3 and 15 cycles of deposition in 1.0 mol L^{-1} H_2SO_4 solution at 1.0 mV s^{-1}.

the cocatalyst. Since surface states can temporarily accumulate charges[31] in the bare Sb_2Se_3 film, the minority carriers that reach the surface states remain trapped and they can recombine or return to their initial energy states. Indeed, this recombination phenomenon is observed in the photocurrent transient profile of Figure 4a (or Figure 4b on a smaller scale) for the bare Sb_2Se_3 film.

According to the reports by Peter, in his work on dynamic aspects of the semiconductor/electrolyte interface in photoelectrochemistry,[32] the exponential decay observed few milliseconds after illumination is switched on due to surface state recombination. Minority carriers trapped in these states capture the majority carriers and recombine until they reach a steady state. Therefore, for the bare Sb_2Se_3 film, the decay profile observed when the material is illuminated can be associated with surface state recombination. For Sb_2Se_3/a-MoS_x films, as long as the surface states are positioned close to the thermodynamic potential for HERs, the presence of the cocatalyst may have led to a decrease in Sb_2Se_3 surface state recombination because it promoted a more efficient charge transfer from these defects to the solution (decrease in the R3 value). Thus, recombination is minimized and the photocurrent transient profile loses decay when illuminated. The pulse profile comparing the recombination of Sb_2Se_3 and Sb_2Se_3/a-MoS_x films is shown in Figure 4c.

When evaluating the values of R4 (related to t_{CB}), the decrease in resistance is also related to the catalytic effect of the MoS_x layer. It is noted that at -0.2 V_{RHE}, the resistance is dramatically decreased for the Sb_2Se_3/a-MoS_x film. This observed effect may be due to a-MoS_x being in its more activated state, that is, with the necessary overpotential to effectively perform the HER, the charge transfer from the valence band starting to be more effective. This effect can be also associated with the deactivation of the surface states recombination at this potential, which makes the photocurrent abruptly increase.[33,34] This behavior is in agreement with the photocurrent observed in these films at -0.2 V_{RHE}, which is the highest value. Although liquid photocurrent is related to all charge transfer processes at the semiconductor/electrolyte interface, the bending of the conduction band to more energetic regions seems to be a crucial factor for photocurrent densities in the presence of the cocatalyst. As also speculated by Tan et al., a-MoS_x needs an additional overpotential to extract the photogenerated electrons at the interface to enable an efficient charge transfer for hydrogen evolution.[19]

In complement, Figure 4a shows the photocurrent transients of the bare Sb_2Se_3 and Sb_2Se_3/a-MoS_x films for an overview of how these films behave at the constant potential in a short period of light and dark. A potential of -0.2 V_{RHE} and 60 s pulses were used, alternating in light and dark. Due to the impossibility of viewing the chronoamperometric profile of the bare Sb_2Se_3 film, Figure 4b shows this film on a smaller scale. Coating Sb_2Se_3 with a-MoS_x allowed a greater current, also in the dark, as the number of deposition cycles increased due to the electrocatalytic effect of MoS_x. This phenomenon is due to several factors involved in the kinetic behavior of the system. Therefore, when the values of dark current of the last pulse transient of the Sb_2Se_3/a-MoS_x films are graphed (Figure 4d), a linear increase can be noted as the number of a-MoS_x deposition cycles increases. In opposite, the photocurrent of the films did not linearly decrease with the number of cycles; an abrupt decrease happened between 9 and 12 cycles. This

https://dx.doi.org/10.1021/acsaem.0c01413
ACS Appl. Energy Mater. XXXX, XXX, XXX−XXX

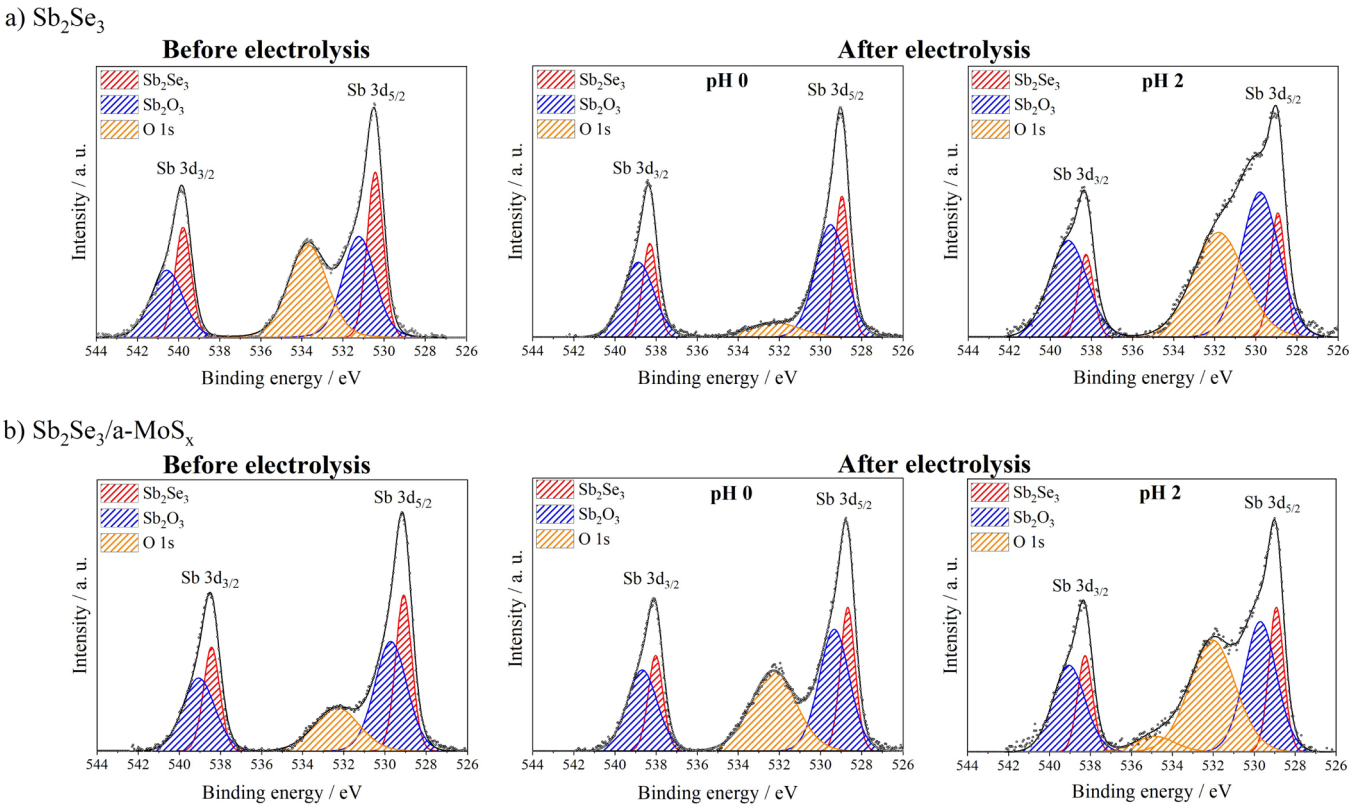

Figure 5. XPS spectra to Sb 3d of (a) bare Sb_2Se_3 films and (b) Sb_2Se_3/a-MoS_x films at pH 0 and 2 before and after electrolysis.

phenomenon makes us believe that the parasitic light absorption effect is not the only cause of the photocurrent reduction as the a-MoS_x layer becomes thicker. A thick cocatalyst film may introduce interface defects that contribute to the decrease in photocurrent, negatively competing with the catalytic benefits.

Polarization curves and Tafel plots were performed to justify the increase in electrocatalytic activity in the dark between Sb_2Se_3/a-MoS_x films obtained from 3 and 15 cycles of deposition, where a considerable increase in the current can be seen between both films (ca. −0.2 and −2.5 mA cm^{-2}, respectively; Figure 4e,f). Coating with a-MoS_x (15 cycles) enabled the reaction to start at a potential ∼50 mV more positive than the a-MoS_x film (3 cycles), implying a higher electrocatalytic activity for HERs. The overpotential at −10 mA cm^{-2} (without *iR* compensation) also revealed a reduction of ∼90 mV for the film with the greatest deposition cycles. Tafel parameter *b* also reveals that the charge is transferred faster at the a-MoS_x (15 cycles) film interface as it has a lower *b* value.[15] This is probably due to the increase in active sites on the a-MoS_x surface associated with the greater number of deposition cycles.

Another interesting behavior observed was that unlike bare Sb_2Se_3, the presence of the cocatalyst also inhibited the photocorrosion of the Sb_2Se_3 film, a problem that we had faced in our previous work.[10,35,36] Unlike recombination processes from decay in each pulse when illuminated, photocorrosion can be observed in current instability for a certain period. The photocurrent for Sb_2Se_3/a-MoS_x films remains more stable at virtually all pulses during illumination (Figure 4a), while the effect of photocorrosion on the Sb_2Se_3 film in the absence of a-MoS_x is noticeable in Figure 4b. This implies that the presence of a-MoS_x was also essential for the inhibition of photocorrosion.

To investigate the phenomenon of photocorrosion that may have harmed the photocurrent of this material, its surface was characterized by XPS before and after electrolysis was performed (Figure 5). The electrolysis was performed at −0.2 V_{RHE} for 30 min in both H_2SO_4 at pH 0 and 0.5 mol L^{-1} Na_2SO_4/H_2SO_4 at pH 2 under illumination to compare the influence of the pH. The main difference observed between the spectra is in the area below the O 1s curve, which implies the formation/dissolution of oxide as a determining factor. Comparing the XPS spectrum of the bare Sb_2Se_3 film before and after electrolysis in pH 0 (Figure 5a), there is a decrease in the peak area corresponding to O 1s. This is likely related to the dissolution of Sb in the forms of $Sb(OH)_2^{2+}$ ions and Sb_2O_3 during photoelectrochemical experiments. As the interfacial pH of the electrode/solution system can increase by a few units during the HER,[37] it has been proposed that reactions 1 to 3 may occur during cathodic scanning in the species formation.[11] When the experiment is done at less acidic pH, this same band increases again due to the precipitation of Sb_2O_3 on the film (only soluble in a strongly acidic or basic medium[38]). With Sb_2Se_3/a-MoS_x (3 cycles) films before and after electrolysis at pH 0 (Figure 5b), the a-MoS_x coating may minimize Sb_2O_3 dissolution, but the increase of the O 1s band can be now associated with the MoO_x formation, which has low acid solubility[38] (details will be discussed later). For this reason, more O 1s states are formed in the spectrum of Figure 5b at pH 2. Therefore, it is likely that Sb_2Se_3 photocorrosion processes are related to the Sb dissolution of the films in an acid medium and, consequently, decrease their photocatalytic activity.

https://dx.doi.org/10.1021/acsaem.0c01413
ACS Appl. Energy Mater. XXXX, XXX, XXX−XXX

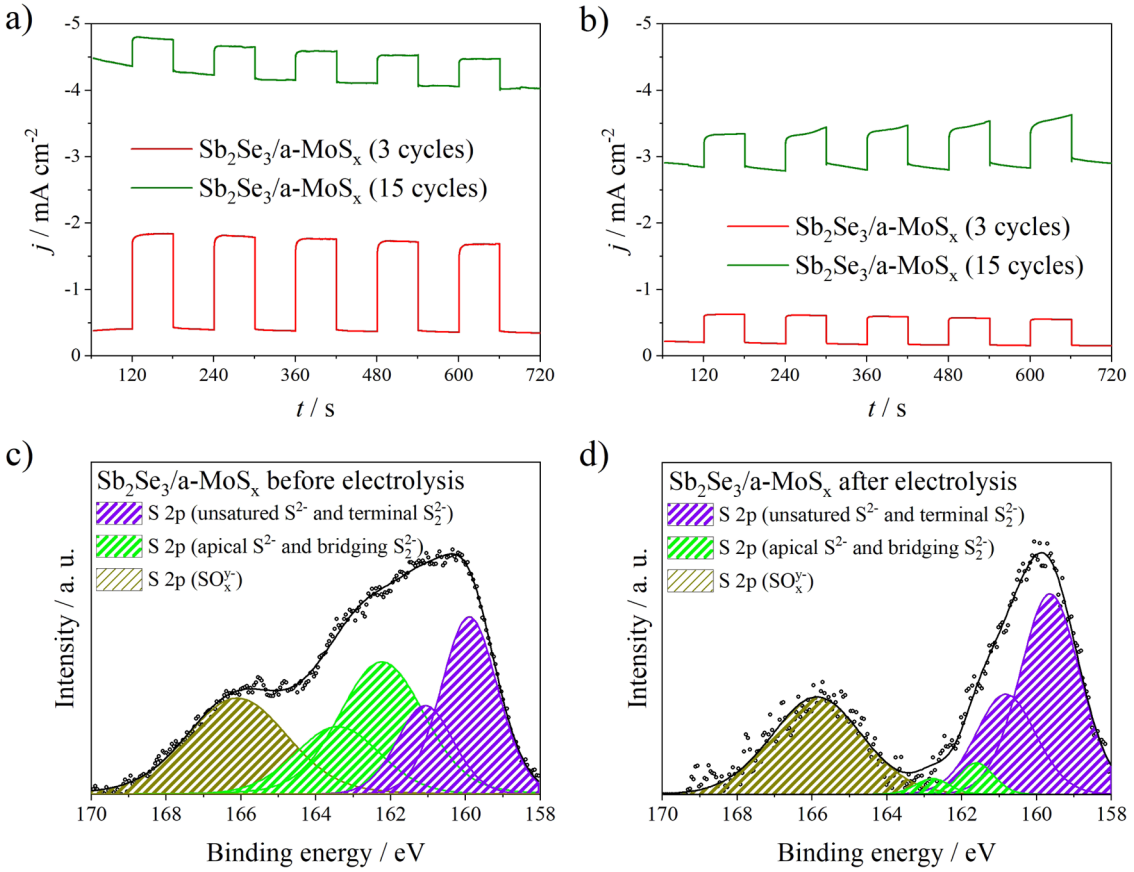

Figure 6. Photocurrent transients (a) before and (b) after potential stress for Sb_2Se_3/a-MoS_x (3 and 15 cycles) films with $E = -0.2$ V_{RHE} and 60 s pulses in light and dark. XPS spectra for Sb_2Se_3/a-MoS_x (3 cycles) film to S 2p (c) before and (d) after illuminated bias.

$$2H_3O^+_{(aq)} + 2e^- \rightarrow H_{2(g)} + 2H_2O_{(l)} \quad (1a)$$

$$2H_2O_{(l)} + 4e^- \rightarrow H_{2(g)} + 2OH^-_{(aq)} \quad (1b)$$

$$Sb_2Se_{3(s)} + 4OH^-_{(aq)} \rightarrow 2Sb(OH)^+_2 + 3Se^{2-}_{(aq)} \quad (2)$$

$$2Sb(OH)^+_2 + 2OH^-_{(aq)} \rightarrow Sb_2O_{3(s)} + 3H_2O_{(l)} \quad (3)$$

To verify the stability of a-MoS_x-coated films toward photocorrosion under potential stress, 300 voltammetric cycles between −0.2 and 0 V_{RHE} were performed under illumination on the same electrolyte used in the photocurrent analysis (Figure S12 in the Supporting Information). After this accelerated stress, the films were again subjected to the photocurrent transient analysis, as previously described, and the transients can be seen in Figure 6a,b. For the Sb_2Se_3/a-MoS_x (3 cycles) film, there is a noticeable decrease of ∼70% in the photocurrent value. This can probably be attributed to the photocorrosion of the exposed Sb_2Se_3 regions. For Sb_2Se_3/a-MoS_x (15 cycles) films, the greater coverage with a-MoS_x attenuates photocorrosion under these conditions. It is also interesting to note that, even though dark current for this film has decreased ∼34%, the photocurrent showed a slight increase.

According to studies by Ting et al. based on turnover frequency (TOF) and density functional theory (DFT),[25] bridging S_2^{2-} present in a-MoS_x provide more active sites for HERs compared with other S atoms belonging to the amorphous structure, such as unsaturated S^{2-}, terminal S_2^{2-}, and apical S^{2-}. However, the S−S bond bridging S_2^{2-} breaks more easily after hydrogen atom adsorption, which may lead to the decreased electrocatalytic effect. In our work, this effect can be confirmed by the decreasing doublet at 162.3 eV of Figure 6c,d of the S 2p spectrum region before and after electrolysis. The XPS spectrum data were processed in the same way as previously reported. However, the S 2p doublets are separated by 1.18 eV,[21] and there is a broad peak corresponding to SO_x^{y-} species.[39] With a greater coverage of a-MoS_x in the 15-cycle deposited film, the effect is more present than that in the 3-cycle deposited film. Furthermore, the slight increase in Sb_2Se_3/a-MoS_x (15 cycles) film photocurrent may also be related to the oxidation of a-MoS_x films during potential stress because the Mo−S bond (S^{2-} unsaturated and S_2^{2-} terminal) has a low binding energy and therefore easily oxidized.[25] As already reported by other authors, molybdenum oxides have *n*-type properties and facilitate the separation of the photogenerated charges through a *p*-*n* junction, which may be also associated with this sudden increase in photocurrent.[40,41] However, it is difficult to distinguish the XPS spectrum between Mo−S and Mo−O bonds. The decrease in absorber coverage is another factor that may be involved since MoO_3 (and other oxidized species) is soluble in a strongly acidic medium,[42] part of the cocatalyst layer may have been dissolved during photoelectrolysis.

Lastly, the films were also subjected to stability testing for 1 h at −0.2 V_{RHE} under constant illumination (100 mW cm^{-2}) and with 30 s pulses every 20 min (Figure S13 in the Supporting Information). Note that over a prolonged period of illumination, the Sb_2Se_3/a-MoS_x (3 cycles) film is unstable and the photocurrent drops 74.5% after 1 h of electrolysis.

https://dx.doi.org/10.1021/acsaem.0c01413
ACS Appl. Energy Mater. XXXX, XXX, XXX−XXX

However, the same does not happen with the film obtained with more deposition cycles although its photocurrent is initially lower than that for the Sb_2Se_3/a-MoS_x (3 cycles) film; there is only a 23.7% drop from the initial value after 1 h of measurement. In other words, there is a competition between high photocurrent and stability due to the Sb_2Se_3 exposed as previously discussed. Although photocurrent values are a comparative parameter when evaluating solar water-splitting systems, stability is an important measure to show long-term viability. In the two stability tests in which the Sb_2Se_3/a-MoS_x system was subjected (cyclic voltammetry and chronoamperometry), it was possible to clearly observe the influence of the a-MoS_x deposition cycle number. Sb_2Se_3/a-MoS_x (15 cycles) proved to be a film with considerable photocurrent and good stability, leading to believe that these all-electrochemically grown films are a good choice for solar water splitting.

CONCLUSIONS

In summary, an Sb_2Se_3/a-MoS_x photocathode was obtained entirely via electrochemical deposition. The effects of the number of a-MoS_x deposition cycles on Sb_2Se_3 was verified in terms of its photoresponse in the HER, charge transfer, and stability in an acid medium. As the number of a-MoS_x deposition cycles increased, the photocurrent decreased due to the nonphotoactive material covering the absorber film and possible interface defects created by the cocatalyst layer. Sb_2Se_3/a-MoS_x films presented an outstanding photocurrent density, ranging from −0.6 to −5.7 mA cm^{-2} in 1 mol L^{-1} H_2SO_4 at −0.2 V_{RHE}, which is between 8 and 70 times higher than the bare Sb_2Se_3. The PEIS analysis and the transient pulse decay showed that there is a reduction in carrier recombination in the Sb_2Se_3 surface states in the presence of a-MoS_x, which may have contributed to its high photocurrent values and minimized the effects of photocorrosion. Furthermore, the XPS analysis before and after electrolysis showed that the presence of the cocatalyst minimizes the dissolution of Sb_2O_3 formed over the Sb_2Se_3 surface. However, the electrolysis favors the breakdown of the S−S bonds responsible for the electrocatalytic effect of a-MoS_x on hydrogen evolution.

ASSOCIATED CONTENT

Supporting Information

The Supporting Information is available free of charge at https://pubs.acs.org/doi/10.1021/acsaem.0c01413.

Experimental Methods; cyclic voltammograms for MoS_x electrodeposition; SEM micrographs; EDS quantification plots; X-ray diffractograms; tables and selenium XPS spectrum data; UV−vis Tauc plots; Mott−Schottky graphs; schematic representation of the band edge position; LSV under solar illumination with 1 s of on/off pulses; EIS equivalent circuit fitting parameters; cyclic voltammograms under constant illumination for accelerated photocorrosion experiments; tests of stability for the different films. (PDF)

AUTHOR INFORMATION

Corresponding Author

Lucia H. Mascaro − *Federal University of São Carlos, São Carlos, São Paulo 13565-905, Brazil;* orcid.org/0000-0001-6908-1097; Email: lmascaro@ufscar.br

Authors

Magno B. Costa − *Federal University of São Carlos, São Carlos, São Paulo 13565-905, Brazil*

Francisco W. S. Lucas − *Department of Chemical and Biological Engineering and Renewable and Sustainable Energy Institute, University of Colorado Boulder, Boulder, Colorado 80309, United States*

Marina Medina − *Federal University of São Carlos, São Carlos, São Paulo 13565-905, Brazil;* orcid.org/0000-0003-0634-3613

Complete contact information is available at: https://pubs.acs.org/10.1021/acsaem.0c01413

Author Contributions

M.B.C. performed the most of writing and experiments under the scientific orientation and writing cooperation of Dr. F.W.S.L. and Dr. L.H.M.

Notes

The authors declare no competing financial interest.

ACKNOWLEDGMENTS

This work was supported by the National Council for Scientific and Technological Development (CNPq) and the São Paulo Research Foundation (FAPESP) (grant #2012/10947-2, grant #2018/16401-8, grant #2017/12794-2, and grant #2017/21365-8), CEPID (grant #2013/07296-2), FAPESP/SHELL (#2017/11986-5), and CAPES finance code 001.

REFERENCES

(1) Zeng, K.; Xue, D.-J.; Tang, J. Antimony Selenide Thin-Film Solar Cells. *Semicond. Sci. Technol.* **2016**, *31*, 1−13.

(2) Patrick, C. E.; Giustino, F. Structural and Electronic Properties of Semiconductor-Sensitized Solar-Cell Interfaces. *Adv. Funct. Mater.* **2011**, *21*, 4663−4667.

(3) Zhang, L.; Li, Y.; Li, C.; Chen, Q.; Zhen, Z.; Jiang, X.; Zhong, M.; Zhang, F.; Zhu, H. Scalable Low-Band-Gap Sb_2Se_3 Thin-Film Photocathodes for Efficient Visible−Near-Infrared Solar Hydrogen Evolution. *ACS Nano* **2017**, *11*, 12753−12763.

(4) Chen, C.; Li, W.; Zhou, Y.; Chen, C.; Luo, M.; Liu, X.; Zeng, K.; Yang, B.; Zhang, C.; Han, J.; Tang, J. Optical Properties of Amorphous and Polycrystalline Sb_2Se_3 Thin Films Prepared by Thermal Evaporation. *Appl. Phys. Lett.* **2015**, *107*, No. 043905.

(5) Isah, K. U.; Yabagi, J. A.; Ahmadu, U.; Kimpa, M. I.; Kana, M. G. Z.; Oberafo, A. A. Effect of Different Copper Precursor Layer Thickness on Properties of Cu_2ZnSnS_4 (CZTS) Thin Films Prepared by Sulfurization of Thermally Deposited Stacked Metallic Layers. *IOSR J. Appl. Phys.* **2013**, *2*, 14−19.

(6) Validžić, I. L.; Mitrić, M.; Abazović, N. D.; Jokić, B. M.; Milošević, A. S.; Popović, Z. S.; Vukajlović, F. R. Structural Analysis, Electronic and Optical Properties of the Synthesized Sb2S3 Nanowires with Small Band Gap. *Semicond. Sci. Technol.* **2014**, *29*, No. 035007.

(7) Yang, B.; Wang, L.; Han, J.; Zhou, Y.; Song, H.; Chen, S.; Zhong, J.; Lv, L.; Niu, D.; Tang, J. $CuSbS_2$ as a Promising Earth-Abundant Photovoltaic Absorber Material: A Combined Theoretical and Experimental Study. *Chem. Mater.* **2014**, *26*, 3135−3143.

(8) Zhou, Y.; Wang, L.; Chen, S.; Qin, S.; Liu, X.; Chen, J.; Xue, D.-J.; Luo, M.; Cao, Y.; Cheng, Y.; Sargent, E. H.; Tang, J. Thin-Film Sb_2Se_3 Photovoltaics with Oriented One-Dimensional Ribbons and Benign Grain Boundaries. *Nat. Photonics* **2015**, *9*, 409−415.

(9) Chen, C.; Bobela, D. C.; Yang, Y.; Lu, S.; Zeng, K.; Ge, C.; Yang, B.; Gao, L.; Zhao, Y.; Beard, M. C.; Tang, J. Characterization of Basic Physical Properties of Sb_2Se_3 and Its Relevance for Photovoltaics. *Front. Optoelectron.* **2017**, *10*, 18−30.

(10) Costa, M. B.; de Souza Lucas, F. W.; Mascaro, L. H. Thermal Treatment Effects on Electrodeposited Sb_2Se_3 Photovoltaic Thin Films. *ChemElectroChem* **2017**, *4*, 2507−2514.
(11) Costa, M. B.; Lucas, F. W. S.; Mascaro, L. H. Improvement of Electrodeposited Sb_2Se_3 Thin Film Photoelectroactivity by Cobalt Grain Boundary Modification. *J. Mater. Chem. A* **2020**, *8*, 13742.
(12) Mali, M. G.; Yoon, H.; Joshi, B. N.; Park, H.; Al-Deyab, S. S.; Lim, D. C.; Ahn, S.; Nervi, C.; Yoon, S. S. Enhanced Photoelectrochemical Solar Water Splitting Using a Platinum-Decorated CIGS/CdS/ZnO Photocathode. *ACS Appl. Mater. Interfaces* **2015**, *7*, 21619−21625.
(13) Chen, T.-Y.; Chang, Y.-H.; Hsu, C.-L.; Wei, K.-H.; Chiang, C.-Y.; Li, L.-J. Comparative Study on MoS_2 and WS_2 for Electrocatalytic Water Splitting. *Int. J. Hydrogen Energy* **2013**, *38*, 12302−12309.
(14) Li, H.; Tsai, C.; Koh, A. L.; Cai, L.; Contryman, A. W.; Fragapane, A. H.; Zhao, J.; Han, H. S.; Manoharan, H. C.; Abild-Pedersen, F.; Nørskov, J. K.; Zheng, X. Activating and Optimizing MoS_2 Basal Planes for Hydrogen Evolution through the Formation of Strained Sulphur Vacancies. *Nat. Mater.* **2016**, *15*, 364−364.
(15) Medina, M.; Corradini, P.; Mascaro, L. H. Facile One-Step Electrodeposition Fabrication of Amorphous MoS_2 Catalysts in Titanium for Hydrogen Evolution Reaction. *J. Braz. Chem. Soc.* **2019**, *00*, 1−9.
(16) Tributsch, H.; Bennett, J. C. Electrochemistry and Photochemistry of MoS_2 Layer Crystals. I. *J. Electroanal. Chem. Interfacial Electrochem.* **1977**, *81*, 97−111.
(17) Britto, R. J.; Benck, J. D.; Young, J. L.; Hahn, C.; Deutsch, T. G.; Jaramillo, T. F. Molybdenum Disulfide as a Protection Layer and Catalyst for Gallium Indium Phosphide Solar Water Splitting Photocathodes. *J. Phys. Chem. Lett.* **2016**, *7*, 2044−2049.
(18) Prabhakar, R. R.; Septina, W.; Siol, S.; Moehl, T.; Wick-Joliat, R.; Tilley, S. D. Photocorrosion-Resistant Sb_2Se_3 Photocathodes with Earth Abundant MoS_x Hydrogen Evolution Catalyst. *J. Mater. Chem. A* **2017**, *5*, 23139−23145.
(19) Tan, J.; Yang, W.; Oh, Y.; Lee, H.; Park, J.; Moon, J. Controlled Electrodeposition of Photoelectrochemically Active Amorphous MoS_x Cocatalyst on Sb_2Se_3 Photocathode. *ACS Appl. Mater. Interfaces* **2018**, *10*, 10898−10908.
(20) Feng, K.; Huang, D.; Li, L.; Wang, K.; Li, J.; Harada, T.; Ikeda, S.; Jiang, F. MoS_x-CdS/Cu_2ZnSnS_4-Based Thin Film Photocathode for Solar Hydrogen Evolution from Water. *Appl. Catal. B Environ.* **2020**, *268*, 118438.
(21) Moulder, J. F.; Stickle, W. F.; Sobol, P. E.; Bomben, K. D. *Handbook of X-Ray Photoelectron Spectroscopy*, 2nd ed.; Chastain, J., Ed.; Perkin-Elmer Corporation: Eden Prairie, 1992.
(22) Liu, X.; Chen, J.; Luo, M.; Leng, M.; Xia, Z.; Zhou, Y.; Qin, S.; Xue, D.-J.; Lv, L.; Huang, H.; Niu, D.; Tang, J. Thermal Evaporation and Characterization of Sb_2Se_3 Thin Film for Substrate Sb_2Se_3/CdS Solar Cells. *ACS Appl. Mater. Interfaces* **2014**, *6*, 10687−10695.
(23) Benck, J. D.; Chen, Z.; Kuritzky, L. Y.; Forman, A. J.; Jaramillo, T. F. Amorphous Molybdenum Sulfide Catalysts for Electrochemical Hydrogen Production: Insights into the Origin of Their Catalytic Activity. *ACS Catal.* **2012**, *2*, 1916−1923.
(24) Jiang, H. Electronic Band Structures of Molybdenum and Tungsten Dichalcogenides by the GW Approach. *J. Phys. Chem. C* **2012**, *116*, 7664−7671.
(25) Ting, L. R. L.; Deng, Y.; Ma, L.; Zhang, Y.-J.; Peterson, A. A.; Yeo, B. S. Catalytic Activities of Sulfur Atoms in Amorphous Molybdenum Sulfide for the Electrochemical Hydrogen Evolution Reaction. *ACS Catal.* **2016**, *6*, 861−867.
(26) Ding, C.; Shi, J.; Wang, Z.; Li, C. Photoelectrocatalytic Water Splitting: Significance of Cocatalysts, Electrolyte, and Interfaces. *ACS Catal.* **2017**, *7*, 675−688.
(27) Yang, J.; Wang, D.; Han, H.; Li, C. Roles of Cocatalysts in Photocatalysis and Photoelectrocatalysis. *Acc. Chem. Res.* **2013**, *46*, 1900−1909.
(28) Bertoluzzi, L.; Bisquert, J. Equivalent Circuit of Electrons and Holes in Thin Semiconductor Films for Photoelectrochemical Water Splitting Applications. *J. Phys. Chem. Lett.* **2012**, *3*, 2517−2522.
(29) Fàbrega, C.; Andreu, T.; Tarancón, A.; Flox, C.; Morata, A.; Calvo-Barrio, L.; Morante, J. R. Optimization of Surface Charge Transfer Processes on Rutile TiO_2 Nanorods Photoanodes for Water Splitting. *Int. J. Hydrogen Energy* **2013**, *38*, 2979−2985.
(30) Heine, V. Theory of Surface States. *Phys. Rev.* **1965**, *138*, A1689−A1696.
(31) Le Formal, F.; Pendlebury, S. R.; Cornuz, M.; Tilley, S. D.; Grätzel, M.; Durrant, J. R. Back Electron−Hole Recombination in Hematite Photoanodes for Water Splitting. *J. Am. Chem. Soc.* **2014**, *136*, 2564−2574.
(32) Peter, L. M. Dynamic Aspects of Semiconductor Photoelectrochemistry. *Chem. Rev.* **1990**, *90*, 753−769.
(33) Zhang, J.; Eslava, S. Understanding Charge Transfer, Defects and Surface States at Hematite Photoanodes. *Sustain. Energy Fuels* **2019**, *3*, 1351−1364.
(34) Yang, X.; Du, C.; Liu, R.; Xie, J.; Wang, D. Balancing Photovoltage Generation and Charge-Transfer Enhancement for Catalyst-Decorated Photoelectrochemical Water Splitting: A Case Study of the Hematite/MnOx Combination. *J. Catal.* **2013**, *304*, 86−91.
(35) Costa, M. B.; Lucas, F. W. S.; Mascaro, L. H. Electrodeposition Conditions Effect Sb_2Se_3 Thin-Film Properties. *ChemElectroChem* **2019**, *6*, 2937−2944.
(36) Costa, M. B.; de Souza Lucas, F. W.; Mascaro, L. H. Electrodeposition of Fe-Doped Sb_2Se_3 Thin Films for Photoelectrochemical Applications and Study of the Doping Effects on Their Properties. *J. Solid State Electrochem.* **2018**, *22*, 1557−1562.
(37) Carneiro-Neto, E. B.; Lopes, M. C.; Pereira, E. C. Simulation of Interfacial pH Changes during Hydrogen Evolution Reaction. *J. Electroanal. Chem.* **2016**, *765*, 92−99.
(38) Larrañaga, M. D.; Lewis, R. J.; Lewis, R. A. *Hawley's Condensed Chemical Dictionary*, 16th ed.; Wiley: Hoboken, 2016.
(39) Escalera-López, D.; Niu, Y.; Park, S. J.; Isaacs, M.; Wilson, K.; Palmer, R. E.; Rees, N. V. Hydrogen Evolution Enhancement of Ultra-Low Loading, Size-Selected Molybdenum Sulfide Nanoclusters by Sulfur Enrichment. *Appl. Catal. B Environ.* **2018**, *235*, 84−91.
(40) Dukštienė, N.; Sinkevičiūtė, D. Photoelectrochemical Properties of MoO_2 Thin Films. *J. Solid State Electrochem.* **2013**, *17*, 1175−1184.
(41) García-García, M.; Colet-Lagrille, M. Electrochemical Fabrication of MoO_2/MoO_3-Based Photo-Anodes for Water Splitting. *ECS Trans.* **2017**, *77*, 77−83.
(42) Saji, V. S.; Lee, C.-W. Molybdenum, Molybdenum Oxides, and Their Electrochemistry. *ChemSusChem* **2012**, *5*, 1146−1161.

https://dx.doi.org/10.1021/acsaem.0c01413
ACS Appl. Energy Mater. XXXX, XXX, XXX−XXX